European Journal of Radiology 121 (2019) 108707

Contents lists available at ScienceDirect

European Journal of Radiology

journal homepage: www.elsevier.com/locate/ejrad

Emerging quantitative MR imaging biomarkers in inflammatory arthritides

Anouk M. Barendregt[a,b,c,e,1,*], Timothy J.P. Bray[d,e,1], Margaret A. Hall-Craggs[d,e,2], Mario Maas[a,b,e,2]

[a] Amsterdam University Medical Centers, location AMC, Department of Radiology and Nuclear Medicine, Meibergdreef 9, 1105 AZ, Amsterdam, the Netherlands
[b] Amsterdam Movement Sciences Research Institute, Amsterdam University Medical Centers, Meibergdreef 9, 1105 AZ, Amsterdam, the Netherlands
[c] Amsterdam University Medical Centers, location AMC, Department of Pediatric Rheumatology, Meibergdreef 9, 1105 AZ, Amsterdam, the Netherlands
[d] Centre for Medical Imaging, University College London, 2nd Floor Charles Bell House, 43-45 Foley Street, W1W 7TS, London, United Kingdom
[e] Department of Radiology, University College London Hospital, 235 Euston Rd, NW12BU, London, United Kingdom

ARTICLE INFO

Keywords:
MRI
Quantification
Arthritis
Osteitis
Cartilage
Synovium

ABSTRACT

Purpose: To review quantitative magnetic resonance imaging (qMRI) methods for imaging inflammation in connective tissues and the skeleton in inflammatory arthritis. This review is designed for a broad audience including radiologists, imaging technologists, rheumatologists and other healthcare professionals.

Methods: We discuss the use of qMRI for imaging skeletal inflammation from both technical and clinical perspectives. We consider how qMRI can be targeted to specific aspects of the pathological process in synovium, cartilage, bone, tendons and entheses. Evidence for the various techniques from studies of both adults and children with inflammatory arthritis is reviewed and critically appraised.

Results: qMRI has the potential to objectively identify, characterize and quantify inflammation of the connective tissues and skeleton in both adult and pediatric patients. Measurements of tissue properties derived using qMRI methods can serve as imaging biomarkers, which are potentially more reproducible and informative than conventional MRI methods. Several qMRI methods are nearing transition into clinical practice and may inform diagnosis and treatment decisions, with the potential to improve patient outcomes.

Conclusions: qMRI enables specific assessment of inflammation in synovium, cartilage, bone, tendons and entheses, and can facilitate a more consistent, personalized approach to diagnosis, characterisation and monitoring of disease.

1. Introduction

The inflammatory arthritides are a broad group of diseases characterised by inflammation of the joints, bones and soft tissues. These diseases result from immune-mediated activation of inflammatory cells and mediators, causing pain, swelling, stiffness and ultimately tissue damage. There have been dramatic improvements in clinical outcome for the inflammatory arthritides [1,2], largely due to the development and clinical introduction of 'biologic' drugs [3,4]. These are complex endogenous molecules that mimic or change the function of the immune system. However, they are expensive and can have serious side effects such as immunosuppression. Not all patients respond to biologic drugs and there are primary and secondary treatment failures. Further, biologics target only inflammatory processes and not the pathways of bone formation [5,6]. Consequently, there is a clinical need for improved treatments and improved methods for diagnosing,

Abbreviations: ADC, apparent diffusion coefficient; Anti-TNF, anti-tumour necrosis factor; AI, artificial intelligence; AIF, arterial input function; BMD, bone mineral density; CSE-MRI, chemical shift-encoded MRI, or also DIXON MRI; DCE-MRI, dynamic contrast-enhanced MRI; dGEMRIC, delayed gadolinium-enhanced MRI of cartilage; DKI, diffusion kurtosis imaging; DWI, diffusion weighted imaging; EES, extracellular space; FF, fat fraction; GAG, glycosaminoglycan; GBCA, gadolinium based contrast agent; IVIM, intravoxel incoherent motion; MCP, metacarpophalangeal; MRI, magnetic resonance imaging; MTX, methotrexate; PDFF, proton density fat fraction; QIB, quantitative imaging biomarker; qMRI, quantitative MRI; QSM, chemical shift-corrected quantitative susceptibility mapping; RA, rheumatoid arthritis; ROI, region of interest; SpA, spondyloarthritis; UTE, ultra-short echo time; ZTE, zero echo time

* Corresponding author at: Amsterdam University Medical Centers, location AMC, Department of Radiology and Nuclear Medicine, Meibergdreef 9, 1105 AZ, Amsterdam, The Netherlands.
E-mail addresses: a.m.barendregt@amsterdamumc.nl (A.M. Barendregt), timothyjpbray@gmail.com (T.J.P. Bray), Margaret.hall-craggs@nhs.net (M.A. Hall-Craggs), m.maas@amc.uva.nl (M. Maas).
[1] These authors contributed equally to this work (shared first authors).
[2] Shared last authors.

https://doi.org/10.1016/j.ejrad.2019.108707
Received 25 June 2019; Received in revised form 14 September 2019; Accepted 9 October 2019

characterizing and monitoring disease, thus supporting more personalised care.

Magnetic resonance imaging (MRI) has emerged as a safe and noninvasive method for evaluating the diverse aspects of the inflammatory process. Recently, quantitative MRI (qMRI) methods have been developed for the measurement of particular physical tissue characteristics, such as cellularity, diffusion, perfusion and fat content, in cartilage, synovium and bone. These characteristics are estimated by acquiring a series of measurements that are sensitized to the properties of the tissues, and then fitting these measurements to a pre-defined model. The ability of qMRI techniques to measure specific tissue characteristics (potentially independent of the hardware and software used to acquire the images) qualifies these measurements to be used as quantitative imaging biomarkers (QIBs) [7]. Sullivan et al. define a QIB as 'an objectively measured imaged characteristic derived from an in vivo image as an indicator of normal biologic processes, pathological processes, or response to a therapeutic intervention' [7].

Importantly, the QIB framework enables rigorous evaluation and/or validation of imaging methods, and there is now a substantial body of literature that can guide the validation process [7–10]. Statistical approaches for measuring the accuracy, precision (including repeatability and reproducibility), biological validity and ultimately clinical utility of candidate QIBs are well-described, meaning that each of these parameters can be assessed within a standardized framework [7–10]. QIB measurements can be compared between scanners, between different hospitals and across time points, and therefore offer greater objectivity than image assessment using conventional MRI. This can reduce the subjectivity associated with conventional MRI assessment and visual scoring approaches commonly used in research [7,11,12]. Further, the use of numeric data in qMRI maps can support automation and machine learning approaches to image analysis [13,14].

The aim of this review is to summarise the current progress in qMRI research applied to inflammation, to discuss how qMRI methods can be used to assess particular tissue processes, and to consider directions for future development of quantitative imaging biomarkers.

2. Pathological considerations

Acute inflammation is the initial response to a harmful stimulus, characterised by movement of plasma and blood cells (leucocytes, particularly granulocytes) into the injured tissue. Acute inflammation increases capillary permeability and blood flow, enabling the movement of plasma fluid, which contains fibrin and immunoglobulins, into the tissue. Increased tissue fluid causes an expansion of the extracellular space and may result in swelling (oedema) of the tissue. In bone where the rigid structure prevents tissue deformity, oedema manifests as a change in the proportional size of each compartment, rather than increased overall tissue size. Vascular stasis can occur and this allows chemical mediators and inflammatory cells to accumulate and respond to the inflammatory insult. Leucocytes migrate into tissue *via* extravasation and these cells perpetuate inflammatory cascades.

Chronic inflammation is the result of a continued response against a persistent insult. In inflammatory arthritides, the 'insult' is loss of tolerance for self-antigens present in the soft tissues. In the chronic phase, the cardinal signs of active inflammation are reduced (but may persist to some extent) and tissue remodeling and fibrosis are initiated. The ultimate result of chronic inflammation varies depending on the disease and anatomical site, but in rheumatic diseases damage to cartilage and the adjacent bone is common. This damage can result in structural lesions that are visible on imaging such as erosions, joint ankylosis and alterations in the structure of subchondral bone.

In rheumatoid arthritis (RA), the prototypic inflammatory arthritis, inflammation typically starts in the synovium, where the activation of inflammatory cells leads to swelling and congestion. Once initiated, the immune response can become chronic, and inflammation becomes amplified in the synovium, resulting in the formation of granulation tissue (pannus), where there is extensive angiogenesis and enzyme production. This causes damage to the adjacent cartilage and bone. In other inflammatory arthritides such as spondyloarthritis (SpA), inflammation may be directed directly against cartilage causing secondary damage to the adjacent bone and soft tissues. The ultimate aim of imaging is to detect and characterize both the active inflammatory process and the structural damage, and to use this information for diagnosis, disease monitoring, prognostication and for guiding treatment.

3. Quantitative MRI techniques used in musculoskeletal imaging

3.1. Diffusion weighted imaging

Diffusion-weighted imaging (DWI) is used to quantify the freedom of water diffusion in tissue. Images are sensitized to diffusion through the addition of motion-sensitizing gradients to a spin echo acquisition; this causes signal loss from moving spins but not from those that are stationary [15–17]. Following acquisition of images with multiple diffusion weightings (b-values [18]), a signal model is fitted to the acquired data, allowing estimation of the diffusion coefficient for the tissue [15–17]. The diffusion coefficient gives an indication of the freedom with which water molecules diffuse. Tissue diffusion is typically estimated using a simple monoexponential model with a single 'apparent' diffusion coefficient (ADC). ADC measurements provide a useful 'summary' measure of tissue diffusion, but there has also been interest in the use of more sophisticated models of diffusion attenuation that can separate the contribution of different tissue characteristics. The intravoxel incoherent motion (IVIM) model, initially proposed by Le-Bihan, can capture both tissue diffusion and a rapid early diffusion component that is believed to be due to tissue perfusion [19–22], whilst diffusion kurtosis imaging (DKI) provides an alternative approach to capturing microstructural complexity [23,24].

The limitations of DWI include relatively low spatial resolution and signal-to-noise ratio. The reproducibility of ADC measurements between different scanners [25–27] and within patients [28] is also relatively poor. Improvements in reproducibility might be achieved by protocol standardization, use of normalized ADC values and use of ADC change over time as outcome measure [26]. ADC measurements may be contaminated by fat in the bone marrow: since fat has a much lower ADC than water, this artificially lowers marrow ADC [29]. Variations in the quality of fat suppression can therefore introduce variability into the measured ADC. Several methods for removing the effect of unsuppressed fat have been proposed, relying on Dixon-like methodology [30,31] which is discussed in more detail later (see Fat-Water MRI). Skeletal maturity also affects ADC measurements of bone marrow [32], but this problem could be addressed by using normal bone as a reference tissue, or by using segmentation methods which account for the variable composition of background marrow.

3.2. Dynamic contrast enhanced imaging

Dynamic contrast-enhanced MRI (DCE-MRI) is a method for measuring tissue perfusion, relying on the acquisition of rapidly repeated images during intravenous administration of gadolinium-based contrast agent (GBCA) [33,34]. The changes in signal intensity over time are analysed to derive maps of specific 'microvascular' parameters. The most widely used model to calculate kinetic parameters from the imaging data was described by Toft and colleagues [35]. In their model, a contrast agent is distributed between two compartments: the tissue and the blood plasma. The model incorporates three standard kinetic parameters: the volume transfer constant between plasma and extracellular space (K^{trans}), the volume of the extracellular space (EES), and the flux rate constant between EES and plasma (K^{ep}) [35]. From these parameters, measures of capillary wall permeability and tissue perfusion can be derived. An essential input function for the Tofts model is the plasma concentration of contrast agent in the arterial system

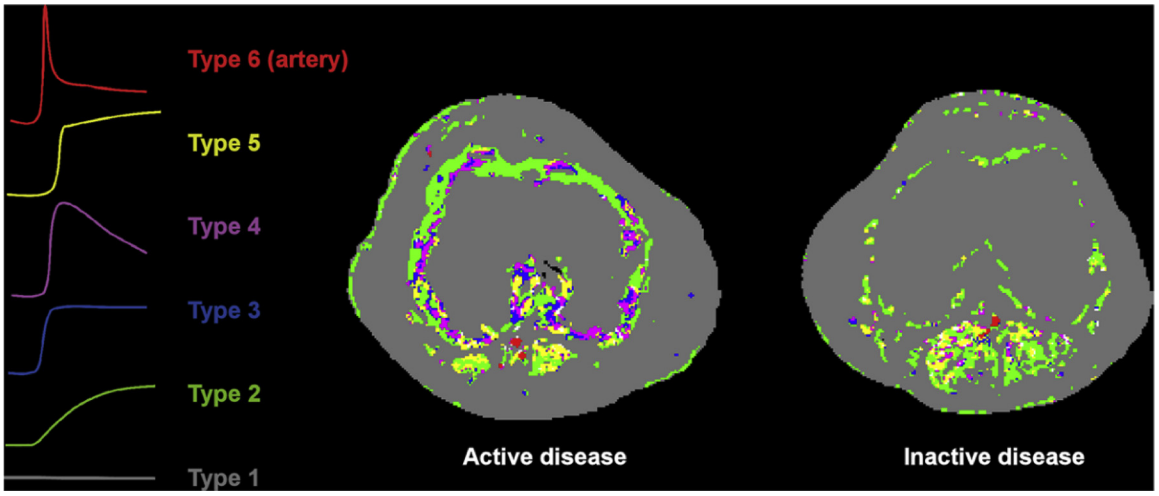

Fig. 1. DCE-derived time intensity curve shape maps of two patients with JIA. The first patient demonstrated active synovial inflammation and the DCE MRI of this patient shows an increased number and percentage of TIC-4 shapes as compared to the second patient, who has no synovial inflammation on MRI. (From Hemke 2014, European Radiology [114]).

supplying the tissue of interest, known as the arterial input function (AIF). Many automated and non-automated methods are available to measure the AIF but obtaining reproducible results has been difficult with most methods [34,36,37]. An alternative approach to DCE-MRI is to analyse the shape of the signal intensity curves of contrast enhancement over time within the tissue of interest (Fig. 1). This approach is often referred to as the descriptive or heuristic method, in which several distinct curve patterns are described (for example: a curve with a rapid enhancement pattern followed by a gradual contrast washout) [34,38]. A description of these curve patterns is often accompanied by measures derived from these curves such as the slope of the enhancement or the maximum enhancement [39].

3.3. T1rho imaging

T1rho (T1ρ) imaging is used to quantify the composition of cartilage. T1ρ is a time constant reflecting spin-lattice relaxation in the rotating frame, and is quantified using a dedicated relaxometry experiment. The magnetization is first flipped into the transverse plane by a 90°radiofrequency pulse. A long, low power radiofrequency pulse (the spin lock pulse) is then applied parallel to the magnetization. The magnetization nutates around the applied spin lock field, but undergoes relaxation (similar to longitudinal relaxation around the B_0 field in the laboratory frame), with time constant T1ρ. T1ρ can be quantified by repeating the experiment with varying duration of the spin lock pulse, and then fitting the known signal model to the acquired data. T1ρ is related to both T1 and T2, and may approach either of these time constants depending on the specific conditions of the experiment. In collagen rich tissues such as cartilage, the main mechanisms contributing to T1ρ are from dipole-dipole interactions and chemical exchange, which inform of the macromolecular content and structure of the cartilage matrix (Fig. 2). Importantly, the experiment can be designed to minimize the dipolar interactions and to emphasise exchange, thus extending the dynamic range of T1ρ compared to T2 and enabling the sequence to accurately detect changes in cartilage structure.

Technical limitations in T1ρ include measurement variability between different scanners and vendors [40]. T1ρ is susceptible to magic angle effects, and correct angulation of the tissue of interest to the B0 field is important [41]. Patient-related factors including obesity and pre-scan exercise can also influence T1ρ values [42,43].

3.4. Delayed gadolinium-enhanced MRI of cartilage

Delayed gadolinium-enhanced MRI of cartilage (dGEMRIC) is used to quantify the composition of cartilage, particularly with respect to glycosaminoglycans (GAGs). Following intravenously administered negatively-charged anionic contrast agent $(Gd(DTPA)^{2-}$ (gadolinium diethylenetriamine-pentaacetic acid), contrast diffuses into cartilage in a dose-dependent manner, but uptake is inhibited by the presence of GAGs, which are negatively charged. Thus, uptake of contrast is inversely related to GAG density. In healthy cartilage, GAGs are abundant. In GAG-depleted joints, such as those affected by arthritis, the net charge of the cartilage matrix increases, and contrast uptake increases. T1 relaxation time can be used to calculate the remaining cartilage GAG concentration [44] expressed as the dGEMRIC index; a shorter dGEMRIC index indicates cartilage damage.

In clinical practice, there are limitations to the use of dGEMRIC. The delay between injection of the contrast agent and the time of optimal imaging is long, substantially prolonging standard imaging protocols. The optimal time interval for imaging is unknown and delays of between 30 and 120 min have been described [45,46] and it is likely that the interval influences the dGEMRIC index. Exercise probably accelerates cartilage uptake of contrast, but the size of this effect is unknown. Finally, there are no studies correlating the histopathological cartilage composition with dGEMRIC values in rheumatic diseases.

3.5. T2 relaxation time mapping

The presence of water in cartilage is dependent on the content and orientation of proteoglycans; T2 relaxation time mapping utilizes this principle to study (amongst others) the zonal orientation of articular cartilage. In T2 mapping, T2 images with different echo times are acquired and, in the simplest case, a monoexponential single model is fit to the data, enabling simple extraction of the relaxation constant T2 for each pixel [47].

An intrinsic limitation of T2 mapping is that T2 measurements can vary depending on the sequence used to acquire the data [48]. A number of complex approaches including the use of extended phase graph modelling have been developed to correct for confounding factors such as the presence of stimulated echoes [49]. Additionally, similar to T1ρ, the angulation of the cartilage towards the main magnetic B0 field influences T2 relaxation time values [50] and loading conditions (exercise, obesity) might influence T2 relaxation values [51,52]. High image resolution is essential for correct delineation of the areas of

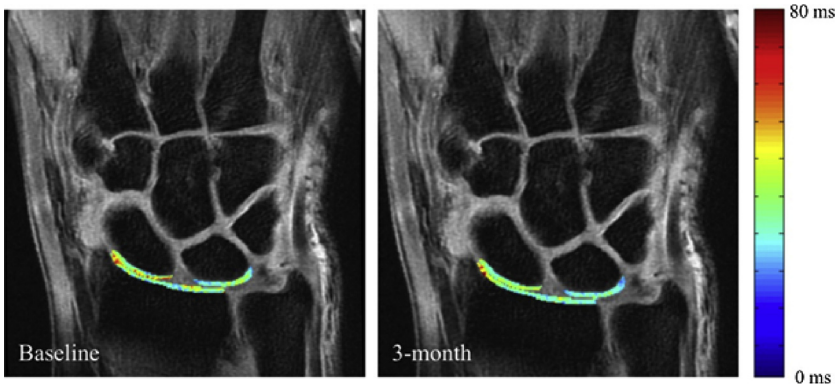

Fig. 2. T1rho of radiocarpal cartilage in an RA patient. The baseline pre-treatment image shows higher T1rho values in the cartilage as compared to the follow-up image, 3 months later. This was a patient with a good clinical response to a treatment regimen of MTX and anti-TNF. (Image from Ku 2016, J Magn Reson Imaging [71]).

interest within the different cartilage layers.

3.6. Fat-Water MRI

Chemical shift-encoded MRI (CSE-MRI or Dixon MRI) utilises the fact that protons in fat and water molecules resonate at slightly different frequencies, depending on variations in the local magnetic field experienced. The Larmor frequency for hydrogen is said to be modified or *shifted* depending on the degree of shielding of the electronic nucleus, which differs between fat and water molecules. Since the MR signal from a voxel containing fat and water is sampled at multiple predetermined time points, the signal can be separated into water and fat components (producing water and fat only images) [53]. The fat fraction (FF) is simply the proportion of the total signal (S) arising from fat [*i.e.* $FF = S_{fat}/(S_{water}+S_{fat})$]. Using modern techniques, it is also possible to eliminate the effect of confounding factors such as T2* and the spectral complexity of fat, which would otherwise bias the FF measurement, thus enabling more accurate quantification [54]. Once relaxation and the spectral complexity of fat have been accounted for, the calculated FF value can be referred to as a proton density fat fraction (PDFF), since it theoretically eliminates these confounds and gives an estimate of the density of fat in the tissue which is independent of the scanner and acquisition parameters used to acquire the data.

3.7. Ultra-short echo time and zero echo time

The tissue components of bones, tendons and entheses are densely packed, causing the MRI signal to decay rapidly. Consequently, alternative methods are needed to image these tissues. Two methods – ultrashort echo time (UTE) and zero echo time (ZTE) - have been developed for capturing the rapidly decaying transverse magnetization of these tissues [55,56]. UTE uses a short radiofrequency excitation pulse with very early read-out gradients; thus tissues with short T2 relaxation times contribute to image signal and contrast.

Limitations of UTE include magic angle effects that can interfere with qualitative and quantitative imaging, especially when tendons or entheses have a multidirectional orientation, preventing the positioning of tendons in an appropriate 'fiber-to-field' angle. In this respect, the Achilles tendon with its unidirectional fiber orientation is well suited to UTE imaging. Another technical issue is eddy currents, which cause image artefacts. Newer protocols such as the 3D-UTE-Cones [57] reduce susceptibility from eddy currents and may require less user input. Despite these issues, UTE/ZTE methods offer a unique opportunity to study these tissues, and provide an alternative window into the inflammatory process.

4. Imaging of synovium

Auto-immune mediated inflammation of the synovial membrane is the hallmark of many of the inflammatory arthritides. Normal synovial membrane has two layers (the subintimal and intimal layer) both comprising a zone of a few cells. After exogenous or endogenous stimulation, the synovial membrane is invaded by inflammatory cells and pro-inflammatory mediators. Consequently, the subintimal and intimal layer thicken due to hyperplasia and hypertrophy of the original synovial lineage cells and the influx of the mononuclear cells. Angiogenesis in the synovial membrane completes the acute inflammatory response. Several quantitative MR techniques can image the cellular and vascular changes in the synovium.

4.1. Quantifying synovial perfusion

DCE imaging can provide a measure of synovial perfusion. Studies of synovial perfusion in inflammatory arthritis have shown that, amongst others, the rate of enhancement and maximum enhancement of contrast influx correlate with histological grades of synovitis ([58–60]. A detailed review of the use of DCE-MRI in inflammatory arthritis has been published recently [34].

4.2. Synovial diffusivity measurement

Studies using DWI in inflammatory arthritis have focused on the differences between diffusivity in synovium and effusion, and between acute and chronic inflammation. Free fluid within a joint effusion typically shows unrestricted diffusion, with high ADC values. Several studies have found that the ADC of synovium in adult or pediatric patients with arthritis is lower than in effusions [61–64]. In these studies ADC of synovium is typically less than $2 \times 10^{-3}\,mm^2/s$ [61,62,64], whereas ADC of effusions was greater than $2 \times 10^{-3}\,mm^2/s$. These studies suggest that ADC values can distinguish synovium from effusion (Fig. 3).

Studies comparing inflamed synovium to non-inflamed synovium are contradictory. Li et al. [63] reported decreasing ADC values with higher grades of inflammation, while Barendregt et al. described higher ADC values in inflamed synovium as compared to non-inflamed synovium [65]. However, the number of patients with synovial inflammation is low in both studies (17 and 31 respectively [63,65]), and larger studies may help characterize inflamed synovium as compared to normal synovium. It could be hypothesized that during acute inflammation, the synovium would have different diffusion properties compared to chronic inflammation. In the chronic inflammatory phase, fibrin deposits in the synovium would reduce water diffusion. Potentially studies correlating ADC with synovial histopathology could help understand the mechanisms affecting synovial ADC.

5. Imaging of cartilage

Cartilage damage is a key feature of inflammatory joint disorders and is caused by pannus invasion and presence of cytokines and proteases in the synovial fluid [66]. Cartilage consists of chondrocytes,

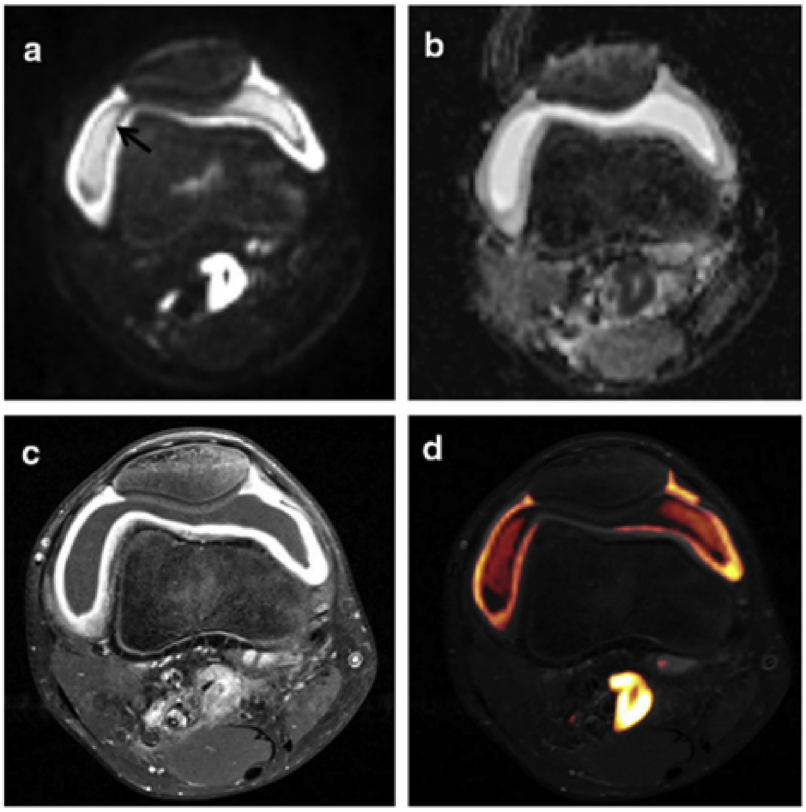

Fig. 3. DWI and ADC in active gonarthritis. DWI with b-value 800 s/mm^2 (a) and $ADC_{50/800}$ map (b) of a 15-year old patient with arthritis of the knee demonstrating higher ADC in effusion as compared to synovium. The post-contrast image (c) shows synovial uptake of contrast agent, note the similarities of delineation of the synovium between the diffusion-derived images and the post-contrast image. (Image from Li 2019, World J Pediatr. 2019 [63]).

collagen and extra-cellular matrix, which contains water, proteoglycans, glycoproteins and lipids. Inflammatory mediators and enzymes affect proteoglycans and collagen; severe degradation of normal proteoglycan and collagen structure and depletion of these molecules occurs after inflammatory stimuli [67]. Conventional MRI can reveal cartilage thinning, fissures and erosion/ulceration, resulting from accumulated microstructural damage to the cartilage matrix. However, early microstructural cartilage damage cannot be visualized on conventional MRI. Other MR tools that can identify early cartilage damage have been developed, but these are not commonly used in clinical practice.

5.1. T1rho (ρ) imaging of cartilage

In 2012, a study of T1rho in five patients with severe and long-standing RA who underwent total knee arthroplasty showed lower T1ρ values in macroscopically normal than in macroscopically abnormal cartilage [68]. In another study, healthy controls without knee symptoms were compared to patients with RA [69]. Patients with RA demonstrated higher T1ρ values in the majority of assessed articular surfaces.

Two studies in RA patients have assessed T1ρ during treatment, and found conflicting results. The first study included 17 symptomatic RA patients and performed MRI of knee cartilage before and 1 year after the start of biological treatment [70]. This study showed that although clinical scores improved after 1 year of treatment, no significant changes in T1ρ values were found in the articular cartilage of the knee [70].

In contrast, in a second study, the radiocarpal cartilage of 9 patients undergoing treatment with methotrexate (MTX) was imaged. Six patients with moderate to severe disease activity started with concomitant anti-tumour necrosis factor (TNF) therapy and 3 patients with low disease activity remained on MTX only [71]. MRI was repeated in all patients after 3 months. After 3 months, good clinical treatment response (as assessed by the EULAR criteria [72]) was observed in 2 patients (both in the MTX + anti-TNF group) and this was associated with declining T1ρ values (Fig. 2), whilst patients with an absent or moderate treatment response showed increasing T1ρ values compared to baseline.

Overall, the evidence for use of cartilage T1ρ to assess treatment response in RA patients is currently inconclusive, and further research in this area is required.

5.2. dGEMRIC imaging

Several authors have studied the use of the dGEMRIC index in patients with RA. Healthy controls have a shorter dGEMRIC index than RA patients [46,73–75]. dGEMRIC indices are lower in patients with long-standing RA compared to recently diagnosed RA [76], indicating the presence of progressive cartilage damage. Metacarpophalangeal joints (MCPs) with the most severe inflammation (highest RAMRIS synovitis score) had lower dGEMRIC indices compared to less severely inflamed MCPs in RA [77,78].

Two small studies investigated changes in dGEMRIC values over time in patients starting treatment. The dGEMRIC index of knee femoral cartilage decreased over time in 7 chronic RA patients started on infliximab but simultaneously taking other regimens (prednisone, azathioprine, MTX) [46]. In a study of 28 patients with early RA who started MTX [78], dGEMRIC indices of MCP 2 and 3 did not significantly change on three sequential MRI scans acquired over 6 months, but the differences in dGEMRIC values between the most severely inflamed MCPs and the less severely inflamed MCPs seemed to decline [78].

5.3. T2 relaxation time mapping

An initial study demonstrated increased T2 relaxation time of knee cartilage in children suffering with JIA compared to healthy controls [79]. In an adult cohort, nine patients with RA and gonarthritis were found to have higher T2 values than healthy volunteers in the articular

cartilage of the knee, except for the cartilage of the patella and lateral tibial plateau [69]. In a recent study in patients with RA, T2 mapping showed that cartilage T2 values of pooled MCP 2 and MCP 3 articular cartilage were significantly higher in patients who had anti-citrullinated protein antibodies as opposed to patients without these antibodies [80], and longer disease duration resulted in higher T2 relaxation time in the articular cartilage. These studies all indicate that the T2 relaxation time is increased in patients with current or previous inflammation, presumably due to an increase in the proportion of 'damaged' proteoglycans.

Interestingly, in a longitudinal analysis of children with JIA, T2 values of the anterior non-weight bearing distal femur were shown to increase over time despite improvements in clinical assessment of disease activity [81]. It was concluded that deterioration of the articular cartilage continued, and that T2 mapping could provide information distinct from that provided by concentional clinical assessment [81]. Unfortunately, no healthy children were assessed in this study and the increase in T2 values over time might have been influenced not only by JIA but also by normal maturation of the cartilage.

6. Imaging of Osteitis

Although osteitis may be seen as a secondary phenomenon in inflammatory disease, it is a central focus of imaging methods that aim to diagnose, stratify and monitor inflammation. The characteristic imaging finding in osteitis is "bone marrow oedema", showing hyperintensity on T2-weighted, fat suppressed images (typically short-tau inversion recovery images), hypointensity on T1-weighted imaging and enhancement with GBCA. These imaging features are probably due to the presence of an inflammatory exudate in tissue, causing increased extracellular fluid and increased numbers of inflammatory cells. Unfortunately, these conventional imaging methods do not correlate specifically to pathological processes and their interpretation is subjective, relying on the expertise and opinion of the observer. qMRI has several potential advantages including more objective and precise assessment of pathology, and an improved ability to monitor change over time.

6.1. Measuring diffusivity in oedematous marrow

In the bone marrow, the presence of an inflammatory exudate causes expansion of the extracellular space, and an increase in the proportion of extracellular water molecules. These extracellular water molecules inhabit a freer, less hindered diffusion environment than intracellular molecules and consequently the ADC increases (Fig. 4). Thus, ADC measurements offer a means to determine the presence and severity of the exudate, reflecting disease activity.

Initial studies of the sacroiliac joint in SpA showed that ADC measurements were increased in areas of bone marrow oedema compared to controls with mechanical back pain [82,83]. Subsequently, it was shown that ADC values reduce after time in patients treated with infliximab, demonstrating biological validity of ADC as a biomarker [84].

DWI had good discriminatory performance for differentiating patients with active inflammation from those without, with potential to inform on treatment response [85]. It has also been shown that ADC measurements can monitor response in young patients with spondyloarthritis [86]. A recent prospective study assessing the utility of ADC as a marker of disease activity in discovertebral lesions showed that a normalised maximum ADC measurement was associated with increased disease activity, functional impairment and functional global assessment [87]. There is also evidence that ADC measurements are higher in inflammatory lesions than inflammatory 'Modic' changes, potentially offering a means to differentiate between these entities [88].

There has been some reluctance to use DWI, and quantitative imaging in general, on the grounds that the process of placing regions of interest (ROIs) is subjective [89]. However, several suggestions have the potential to resolve these issues [90]. Automated methods for ROI placement using histographic analysis to 'target' the inflamed parts of the ADC distribution may improve the sensitivity of this biomarker for active inflammation [91].

As ADC is essentially a 'summary' measure of tissue diffusion, there has been interest in the use of more sophisticated models of diffusion attenuation such as IVIM and DKI [19–22]. DKI aims to capture the microstructural complexity in marrow and preliminary data suggest potential improvements in diagnostic performance [92]. Preliminary data also suggest that IVIM offers a better description of the signal in both normal and inflamed marrow than the monoexponential ADC model or kurtosis, suggesting that this model deserves further investigation (Fig. 5) [93].

6.2. Quantifying fat in the marrow

CSE-MRI/PDFF imaging can quantify bone marrow fat fraction, reflecting bone inflammation. A strength of PDFF as a biomarker is its reproducibility across scanners and vendors [94,95]. It can also quantify both active and chronic inflammation, facilitating more detailed assessment of the heterogenous nature of inflammation.

CSE-MRI imaging in young patients with spondyloarthritis has shown that PDFF measurements are significantly reduced in areas of bone marrow oedema compared to normal marrow (which has a PDFF

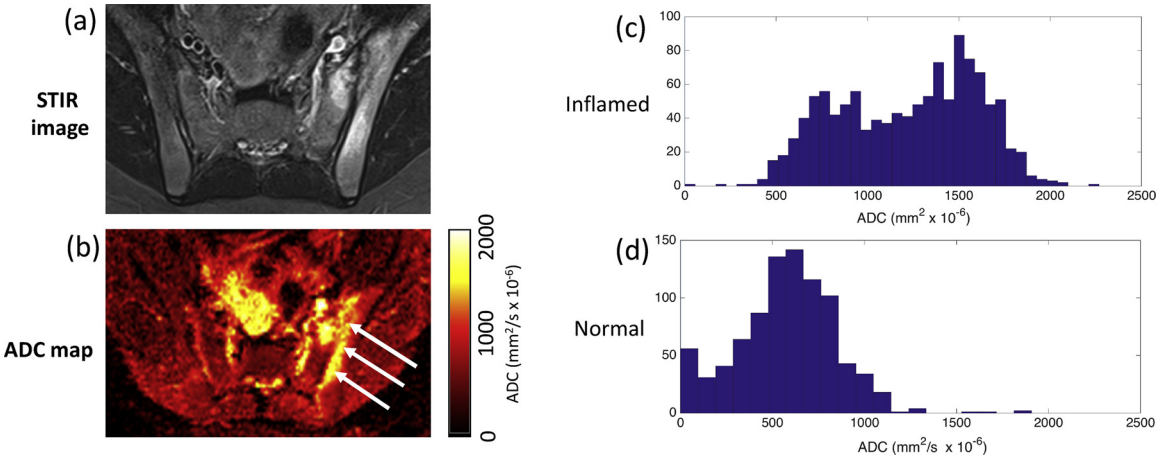

Fig. 4. ADC mapping in a patient with sacroiliitis. A conventional STIR image is shown in (a); the corresponding ADC map is shown in (b). The arrows indicate areas of bone marrow oedema, corresponding to the high signal on the STIR image. (c,d) show ADC histograms derived from subchondral bone in a patient with sacroiliitis and a control respectively; (c) demonstrates the rightward shift in ADC values in the inflamed subject.

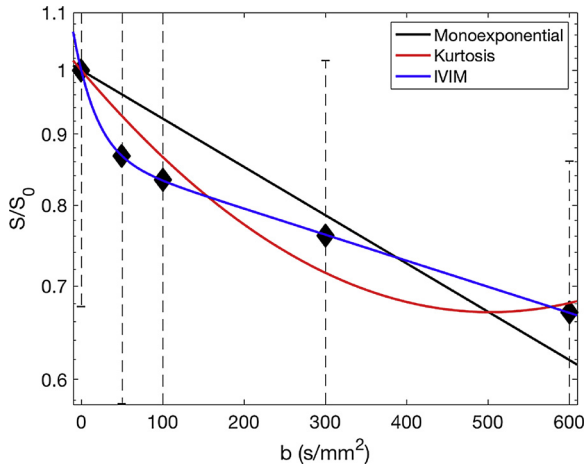

Fig. 5. Diffusion-weighted signal in normal and inflamed marrow. Signal intensity is shown on a log scale on the y axis, b-value is shown on the x-axis. The datapoints are shown as triangles and the error bars indicate the standard deviation. The IVIM model (blue) provides the best description of the data at the lower b-values; the other models cannot capture the early 'perfusion' component of the IVIM signal.

of around 50%), and significantly increased in areas of fat metaplasia (thought to reflect previous inflammation) (Fig. 6) [96]. PDFF measurements may also be useful as a biomarker of structural damage [97], and can distinguish patients with 'inactive' sacroiliitis from healthy controls [98]. Histographic measurements can be used to quantify changes in PDFF and could enable a more sensitive and specific assessment of qMRI maps in clinical practice [91].

CSE-MRI may also be used to correct for the effects of chemical shift where it would otherwise confound measurements of tissue properties. For example, chemical shift-corrected quantitative susceptibility mapping (QSM) has shown some promising results in the quantification of bone mineral density (BMD) in phantoms (see below) [99]. CSE-MRI methods can be combined with techniques for T2-mapping, enabling a specific measurement of the T2 of the water resonance alone without contamination from the T2 of fat [100]. This approach has shown promise in muscle [101].

6.3. Quantifying marrow perfusion

Using perfusion imaging, it may be possible to detect subtle derangements in tissue vasculature, and to separate these from the increase in extracellular water (which probably dominates the MR characteristics of the tissue). There have been some early studies investigating this issue in the marrow surrounding the sacroiliac joints. Perfusion parameters K^{trans}, K^{ep}, V^{e}, time to peak (TTP) and maximum concentration have been shown to differentiate between patients with active and inactive SpA stratified using clinical and biochemical criteria [102]. Potentially DCE-MRI could monitor changes in inflammation with biologic therapy [84]. An interesting possibility is that IVIM diffusion models may offer an alternative means to probe tissue diffusion. For example, the rapid diffusion parameter Df, correlates with the maximum enhancement of tissue, arguing that this parameter reflects tissue perfusion [22]. However, more confirmatory data are needed.

6.4. Measurement of bone formation and loss

The spondyloarthritides are characterised by changes in the bone structure and bone mineral density, both in the form of new bone formation (which contributes to joint fusion and the eventual development of the characteristic 'bamboo spine') and osteoporosis. Early new bone formation and bone loss can be subtle and difficult to detect using conventional sequences.

Measurement of R2* - the rate of signal decay in a gradient echo sequence – is correlated with bone mineral density, and preliminary data have shown that R2* measurements are reduced in areas of fat metaplasia, potentially providing a mechanism to monitor BMD (Fig. 7) [96]. QSM can also detect changes in BMD in phantoms, although data from patients are equivocal [99]. R2* mapping and QSM measurements rely on local dephasing produced by variations in the amount of mineral present in the tissue. An important technical consideration is that both methods can be confounded by variations in tissue fat content but this can be more easily corrected for with QSM [99].

An alternative approach to imaging bone mineral component is to use ultrashort echo time (UTE) and zero echo time (ZTE) imaging. UTE and ZTE methods can acquire signal from water molecules within the cortex and trabeculae themselves, and thus inform on the structure/porosity of bone [56,103–105].

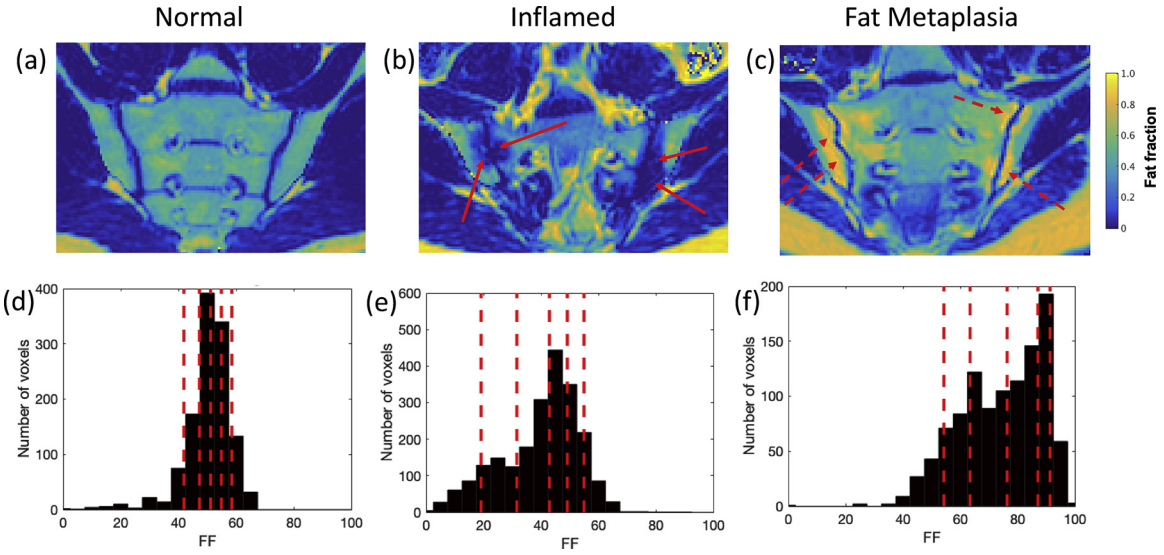

Fig. 6. Image of osteitis with chemical shift-encoded MRI. Fat fraction maps are shown on the top row (a,b,c) and the corresponding histograms are below (d,e,f). In the inflamed case (b,e), areas of bone marrow oedema produce reduced fat fraction measurements. In areas of fat metaplasia (c,f), fat fraction measurements are increased.

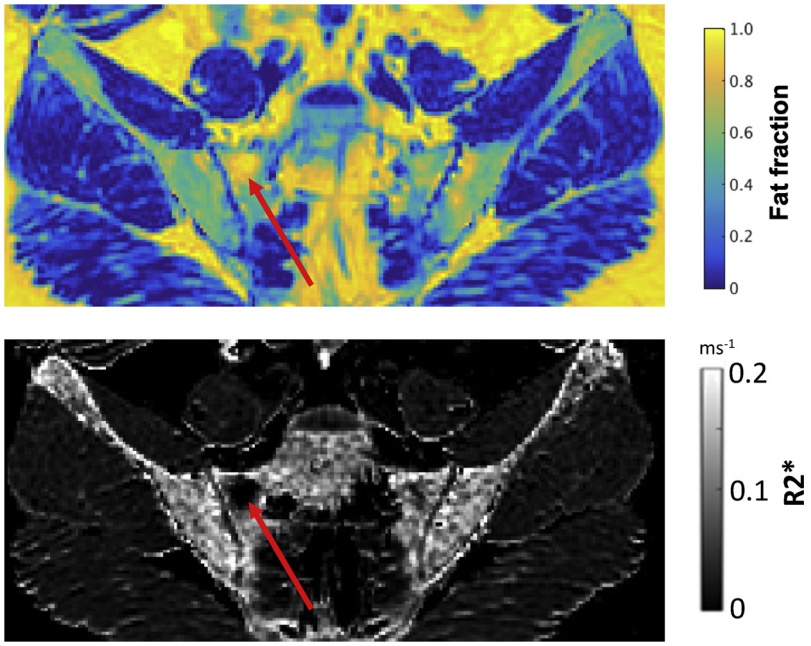

Fig. 7. Fat fraction and R2* maps showing fat metaplasia. The arrow shows an area of fat metaplasia (a post-inflammatory lesion characterised by increased marrow lipid content), with increased fat fraction measurements (a) and reduced R2* measurements (b).

7. Imaging of tendons and entheses

Tendons and entheses can be involved in the disease process in all inflammatory arthritides, however entheseal involvement is particularly common in SpA [106]. Tendons and entheses consist of tightly packed collagen fibers that connect connective tissues originating from the musculoskeletal apparatus (such as tendon, ligaments and fascia) to bone. Interstitial volume and water content are low in these tissues. Consequently, on conventional MRI, entheseal abnormalities are only seen when a significant disruption of the normal fibrillary structure is present, when water accumulates inside a tendon, or when a tendon thickens. These findings are considered as major abnormalities. Earlier signs of tendon and/or enthesis pathology are difficult to detect due to the very short T2 (1–2 ms) of normal entheses and tendons and are likely overlooked by conventional MRI (Fig. 8). Consequently, imaging which captures echos early in the imaging experiment (such as UTE and ZTE), has been utilized for imaging these dense, collagen rich structures.

Preliminary data [107] indicated that UTE images of patients with psoriatic arthritis showed many entheseal abnormalities not captured on conventional T1-weighted and T2-weighted images. In a further study of 25 patients with SpA, abnormalities in the Achilles tendon were more commonly seen on contrast enhanced UTE and 3D spoiled gradient echo with a TE of 2 ms than on conventional MRI or ultrasound [108]. The authors also imaged 10 healthy controls and found abnormalities on MRI in only 1 patient (10%), while in the SpA group, up to 92% of patients demonstrated abnormalities on MRI. In another study, UTE was used as a technique to quantify enhancement in the enthesis [109]. Twenty-four symptomatic SpA-patients and 14 healthy controls underwent UTE (TE = 0.07 ms) before and after GBCA administration. Quantification was performed by calculating the relative contrast enhancement in a single-slice axial ROI of the Achilles tendon. Relative enhancement on the UTE images was higher in SpA patients as compared to controls.

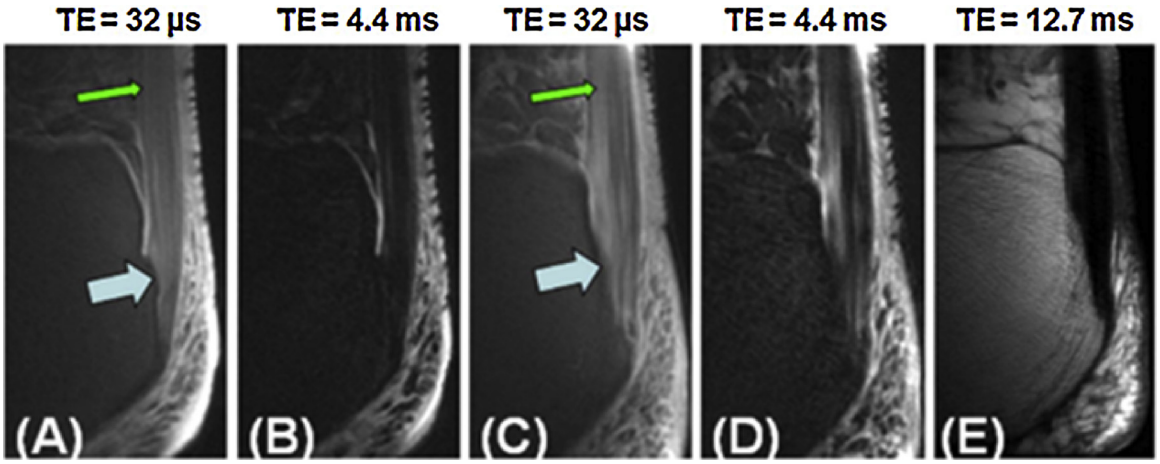

Fig. 8. UTE imaging of the Achilles tendon. UTE images of a healthy volunteer (a, b) and a patient with psoriatic arthritis (c, d) show the increase in signal and visibility of the tendon structure with lower echo times. Note the heterogeneously increased signal in the posterior half of the Achilles tendon in the patient on the 32 us image. On the conventional T1-FSE image (e) the tendon abnormalities seem less extensive. (Image from Chen 2018 [57]).

8. Future directions

One of the major goals for future research will be to translate qMRI techniques into clinical practice. Although many of these techniques are promising, the time taken to acquire the images and requirement for offline processing will need to be addressed before these methods can be widely implemented. Some of the faster techniques (*e.g.* diffusion and Dixon imaging) are relatively easy to implement and are being used in some centres. Accelerated acquisition and relaxometry techniques aiming to separate individual properties of tissue may help to overcome some of the technical challenges, and to increase the uptake of these methods. The methods will also need large-scale collaborative validation studies to demonstrate repeatability, reproducibility and clinical benefit. Furthermore, the clinical implementation of qMRI techniques will require the engagement of all members of multidisciplinary teams involved in patient care.

An interesting new development is the use of qMRI to image immune cell function and metabolism at inflamed sites. There has been preclinical research demonstrating that inflammatory cells can be magnetically labelled and tracked in vivo, with promising results in rodent models of inflammation [110,111]. Hyperpolarised MRI can potentially be used to detect inflammation-induced hypoxia: rats with a model of inflammatory arthritis have been injected with 13C-pyruvate and an increase in labelled 13C-labelled pyruvate and in the lactate pyruvate ratio in inflamed tissue has been shown [112]. Given the recent advances in oncological imaging, where hyperpolarised MRI has been used to image small numbers of human subjects, it seems possible that this method could be applied to inflammatory diseases.

Recent, rapid advances in artificial intelligence (AI) are an important development [14,113]. Although extensive training and refinement of AI algorithms is required before it can be incorporated into research and clinical practice, we expect that AI will ultimately facilitate automated assessment and scoring of quantitative images. Training of these algorithms may require large, international collaborations to acquire datasets of sufficient size. Also, a coordinated effort is needed to ensure that methods are implemented in a consistent, transparent fashion between different centres, particularly where the vendors of MRI scanners may vary.

An outstanding clinical problem is differentiating between diseases which are primarily inflammatory and those where inflammation is secondary to another insult. 'Bone marrow oedema' has been used as a descriptive term for bone marrow signals changes for many years; despite evidence that this lesion is highly heterogenous, it remains poorly characterised in clinical practice. Similarly, synovial inflammation in inflammatory arthritis might be difficult to differentiate from synovial inflammation resulting from biomechanical damage. qMRI techniques may facilitate more detailed phenotyping of these changes and help differentiate inflammatory from non-inflammatory causes of arthritis.

9. Summary

There have been significant advances in recent years in the imaging and quantification of inflammation of the musculoskeletal system. Acute and chronic inflammation in cartilage, synovium, bone marrow and tendons can be measured with qMRI and these detailed quantitative imaging biomarkers can potentially impact patient care. Improvements in imaging technology have been paralleled by newer drugs, particularly biologic therapies. The challenge is to marry these developments and to produce imaging biomarkers, which are clinically practical, biologically relevant, and enable us to tailor our treatments to patients in the clinic.

Acknowledgement

MHC receives funding from the University College London Hospitals, UK National Institute for Health Research (NIHR) Biomedical Research Centre.

References

[1] S. Ajeganova, T. Huizinga, Sustained remission in rheumatoid arthritis: latest evidence and clinical considerations, Ther. Adv. Musculoskelet. Dis. 9 (2017) 249–262, https://doi.org/10.1177/1759720X17720366.
[2] W. Kievit, J. Fransen, M.C. de Waal Malefijt, A.A. den Broeder, P.L.C.M. van Riel, Treatment changes and improved outcomes in RA: an overview of a large inception cohort from 1989 to 2009, Rheumatol. (United Kingdom). 52 (2013) 1500–1508, https://doi.org/10.1093/rheumatology/ket166.
[3] A. Jones, C. Ciurtin, M. Ismajli, M. Leandro, R. Sengupta, P.M. Machado, Biologics for treating axial spondyloarthritis, Expert Opin. Biol. Ther. 7 (2018) 641–652, https://doi.org/10.1080/14712598.2018.1468884.
[4] J.S. Smolen, R. Landewé, J. Bijlsma, G. Burmester, K. Chatzidionysiou, M. Dougados, J. Nam, S. Ramiro, M. Voshaar, R. van Vollenhoven, D. Aletaha, M. Aringer, M. Boers, C.D. Buckley, F. Buttgereit, V. Bykerk, M. Cardiel, B. Combe, M. Cutolo, Y. van Eijk-Hustings, P. Emery, A. Finckh, C. Gabay, J. Gomez-Reino, L. Gossec, J.-E. Gottenberg, J.M.W. Hazes, T. Huizinga, M. Jani, D. Karateev, M. Kouloumas, T. Kvien, Z. Li, X. Mariette, I. McInnes, E. Mysler, P. Nash, K. Pavelka, G. Poór, C. Richez, P. van Riel, A. Rubbert-Roth, K. Saag, J. da Silva, T. Stamm, T. Takeuchi, R. Westhovens, M. de Wit, D. van der Heijde, EULAR recommendations for the management of rheumatoid arthritis with synthetic and biological disease-modifying antirheumatic drugs: 2016 update, Ann. Rheum. Dis. 76 (6) (2017) 960–977, https://doi.org/10.1136/annrheumdis-2016-210715.
[5] D. Wendling, P. Claudepierre, New bone formation in axial spondyloarthritis, Jt. Bone Spine. 80 (2013) 454–458, https://doi.org/10.1016/j.jbspin.2013.02.004.
[6] T.J.P. Bray, A. Lopes, C. Fisher, C. Ciurtin, D. Sen, M.A. Hall-Craggs, Sacroiliac joint ankylosis in young spondyloarthritis patients receiving biologic therapy: observation of serial magnetic resonance imaging scans, Arthritis Rheumatol. 71 (4) (2019) 594–598, https://doi.org/10.1002/art.40750.
[7] D.C. Sullivan, N.A. Obuchowski, L.G. Kessler, D.L. Raunig, C. Gatsonis, M. Kondratovich, L.M. Mcshane, A.P. Reeves, D.P. Barboriak, R.L. Wahl, Metrology standards for quantitative imaging, Radiology 277 (2015) 813–825, https://doi.org/10.1148/radiol.2015142202.
[8] N.A. Obuchowski, A.P. Reeves, E.P. Huang, X. Wang, A.J. Buckler, H.J.G. Kim, H.X. Barnhart, E.F. Jackson, M.L. Giger, G. Pennello, A.Y. Toledano, J. Kalpathy-Cramer, T.V. Apanasovich, P.E. Kinahan, K.J. Myers, D.B. Goldgof, D.P. Barboriak, R.J. Gillies, L.H. Schwartz, D.C. Sullivan, Quantitative imaging biomarkers: a review of statistical methods for computer algorithm comparisons, Stat. Methods Med. Res. 24 (2014) 68–106, https://doi.org/10.1177/0962280214537390.
[9] N.A. Obuchowski, H.X. Barnhart, A.J. Buckler, G. Pennello, X.-F. Wang, J. Kalpathy-Cramer, H.J.G. Kim, A.P. Reeves, Statistical issues in the comparison of quantitative imaging biomarker algorithms using pulmonary nodule volume as an example, Stat. Methods Med. Res. 24 (2015) 107–140, https://doi.org/10.1177/0962280214537392.
[10] J.P.B. O'Connor, E.O. Aboagye, J.E. Adams, H.J.W.L. Aerts, S.F. Barrington, A.J. Beer, R. Boellaard, S.E. Bohndiek, M. Brady, G. Brown, D.L. Buckley, T.L. Chenevert, L.P. Clarke, S. Collette, G.J. Cook, N.M. Desouza, J.C. Dickson, C. Dive, J.L. Evelhoch, C. Faivre-Finn, F.A. Gallagher, F.J. Gilbert, R.J. Gillies, V. Goh, J.R. Griffiths, A.M. Groves, S. Halligan, A.L. Harris, D.J. Hawkes, O.S. Hoekstra, E.P. Huang, B.F. Hutton, E.F. Jackson, G.C. Jayson, A. Jones, D.M. Koh, D. Lacombe, P. Lambin, N. Lassau, M.O. Leach, T.Y. Lee, E.L. Leen, J.S. Lewis, Y. Liu, M.F. Lythgoe, P. Manoharan, R.J. Maxwell, K.A. Miles, B. Morgan, S. Morris, T. Ng, A.R. Padhani, G.J.M. Parker, M. Partridge, A.P. Pathak, A.C. Peet, S. Punwani, A.R. Reynolds, S.P. Robinson, L.K. Shankar, R.A. Sharma, D. Soloviev, S. Stroobants, D.C. Sullivan, S.A. Taylor, P.S. Tofts, G.M. Tozer, M. Van Herk, S. Walker-Samuel, J. Wason, K.J. Williams, P. Workman, T.E. Yankeelov, K.M. Brindle, L.M. McShane, A. Jackson, J.C. Waterton, Imaging biomarker roadmap for cancer studies, Nat. Rev. Clin. Oncol. 14 (2017) 169–186, https://doi.org/10.1038/nrclinonc.2016.162.
[11] M.A. Hall-Craggs, T.J.P. Bray, C. Ciurtin, A. Bainbridge, Quantitative magnetic resonance imaging has potential for assessment of spondyloarthritis: Arguments for its study and use, J. Rheumatol. 46 (2019) 541–542, https://doi.org/10.3899/jrheum.181049.
[12] P. Tofts, Quantitative MRI of the Brain: Measuring Changes Caused by Disease, (2005), https://doi.org/10.1002/0470869526.
[13] M.L. Giger, Machine learning in medical imaging, J. Am. Coll. Radiol. 15 (2018) 512–520, https://doi.org/10.1016/j.jacr.2017.12.028.
[14] G. Chartrand, P.M. Cheng, E. Vorontsov, M. Drozdzal, S. Turcotte, C.J. Pal, S. Kadoury, A. Tang, Deep learning: a primer for radiologists, RadioGraphics 37 (2017) 2113–2131, https://doi.org/10.1148/rg.2017170077.
[15] D. Le Bihan, Apparent diffusion coefficient and beyond: what diffusion MR imaging can tell us about tissue structure, Radiology 268 (2013) 318–322, https://doi.org/10.1148/radiol.13130420.
[16] D. Le Bihan, What can we see with IVIM MRI? Neuroimage 187 (2018) 56–67, https://doi.org/10.1016/j.neuroimage.2017.12.062.
[17] M.A. Bernstein, K.E. King, X.J.X.Y. Zhou, W. Fong, Handbook of MRI pulse sequences, Med. Phys. 32 (2005) 1452, https://doi.org/10.1118/1.1904597.
[18] D. Le Bihan, R. Turner, C.T. Moonen, J. Pekar, Imaging of diffusion and microcirculation with gradient sensitization: design, strategy, and significance, J. Magn. Reson. Imaging 1 (1991) 7–28, https://doi.org/10.1002/jmri.1880010103.
[19] H. Sun, K. Liu, H. Liu, Z. Ji, Y. Yan, L. Jiang, J. Zhou, Comparison of bi-exponential and mono-exponential models of diffusion-weighted imaging for detecting active sacroiliitis in ankylosing spondylitis, Acta radiol. 59 (2017) 468–477, https://doi.

org/10.1177/0284185117722811.
[20] Y.H. Zhao, S.L. Li, Z.Y. Liu, X. Chen, X.C. Zhao, S.Y. Hu, Z.H. Liu, S.Y. M, Q. Chan, C.H. Liang, Detection of active sacroiliitis with ankylosing spondylitis through intravoxel incoherent motion diffusion-weighted MR imaging, Eur. Radiol. 25 (2015) 2754–2763, https://doi.org/10.1007/s00330-015-3634-2.
[21] S. Wang, Y. Gao, G. Liu, F. Xiao, J. Zhao, Research on musculoskeletal model of elbow joint for evaluating the feasibility of FES, Biomed. Mater. Eng. 26 (Suppl. 1) (2015) S593–S600, https://doi.org/10.3233/BME-151350.
[22] Y. Zhao, Q. Zhang, W. Li, Y. Feng, Y. Guo, Z. Xiang, S. Li, Assessment of Correlation between Intravoxel Incoherent Motion Diffusion Weighted MR Imaging and Dynamic Contrast-Enhanced MR Imaging of Sacroiliitis with Ankylosing Spondylitis, Biomed Res. Int. 2017 (2017) 1–9, https://doi.org/10.1155/2017/8135863.
[23] J.H. Jensen, J.A. Helpern, A. Ramani, H. Lu, K. Kaczynski, Diffusional kurtosis imaging: The quantification of non-Gaussian water diffusion by means of magnetic resonance imaging, Magn. Reson. Med. 53 (2005) 1432–1440, https://doi.org/10.1002/mrm.20508.
[24] J.H. Jensen, J.A. Helpern, MRI quantification of non-Gaussian water diffusion by kurtosis analysis, NMR Biomed. 23 (2010) 698–710, https://doi.org/10.1002/nbm.1518.
[25] M. Sasaki, K. Yamada, Y. Watanabe, M. Matsui, Variability in absolute apparent diffusion coefficient values across different platforms may Be substantial: a multivendor, multi-institutional comparison study, Radiology 249 (2008) 624–630, https://doi.org/10.1148/radiol.2492071681.
[26] F.C. Schmeel, Variability in quantitative diffusion-weighted MR imaging (DWI) across different scanners and imaging sites: is there a potential consensus that can help reducing the limits of expected bias? Eur. Radiol. 29 (2019) 2243–2245, https://doi.org/10.1007/s00330-018-5866-4.
[27] B. Taouli, A.J. Beer, T. Chenevert, D. Collins, C. Lehman, C. Matos, A.R. Padhani, A.B. Rosenkrantz, A. Shukla-Dave, E. Sigmund, L. Tanenbaum, H. Thoeny, I. Thomassin-Naggara, S. Barbieri, I. Corcuera-Solano, M. Orton, S.C. Partridge, D.M. Koh, Diffusion-weighted imaging outside the brain: consensus statement from an ISMRM-sponsored workshop, J. Magn. Reson. Imaging 44 (2016) 521–540, https://doi.org/10.1002/jmri.25196.
[28] A.C. Braithwaite, B.M. Dale, D.T. Boll, E.M. Merkle, Short- and midterm reproducibility of apparent diffusion coefficient measurements at 3.0-T diffusion-weighted imaging of the abdomen, Radiology 250 (2009) 459–465, https://doi.org/10.1148/radiol.2502080849.
[29] O. Dietrich, T. Geith, M.F. Reiser, A. Baur-Melnyk, Diffusion imaging of the vertebral bone marrow, NMR Biomed. 30 (2017) e3333, https://doi.org/10.1002/nbm.3333.
[30] D. Hernando, D.C. Karampinos, K.F. King, J.P. Haldar, S. Majumdar, J.G. Georgiadis, Z.P. Liang, Removal of olefinic fat chemical shift artifact in diffusion MRI, Magn. Reson. Med. 65 (2011) 692–701, https://doi.org/10.1002/mrm.22670.
[31] J. Burakiewicz, M.T. Hooijmans, A.G. Webb, J.J.G.M. Verschuuren, E.H. Niks, H.E. Kan, Improved olefinic fat suppression in skeletal muscle DTI using a magnitude-based dixon method, Magn. Reson. Med. 79 (2018) 152–159, https://doi.org/10.1002/mrm.26655.
[32] T.J. Bray, K. Vendhan, J. Roberts, D. Atkinson, S. Punwani, D. Sen, Y. Ioannou, M.A. Hall-Craggs, Association of the apparent diffusion coefficient with maturity in adolescent sacroiliac joints, J. Magn. Reson. Imaging 44 (2016) 556–564, https://doi.org/10.1002/jmri.25209.
[33] J.P.B. O'Connor, P.S. Tofts, K.A. Miles, L.M. Parkes, G. Thompson, A. Jackson, Dynamic contrast-enhanced imaging techniques: CT and MRI, Br. J. Radiol. 84 (2) (2011) S112–S120, https://doi.org/10.1259/bjr/55166688.
[34] M. Boesen, O. Kubassova, I. Sudol-Szopinska, M. Maas, P. Hansen, J.D. Nybing, E.H. Oei, R. Hemke, A. Guermazi, MR imaging of joint infection and inflammation with emphasis on dynamic contrast-enhanced MR imaging, PET Clin. 13 (2018) 523–550, https://doi.org/10.1016/j.cpet.2018.05.007.
[35] P.S. Tofts, G. Brix, D.L. Buckley, J.L. Evelhoch, E. Henderson, M.V. Knopp, H.B. Larsson, T.Y. Lee, N.A. Mayr, G.J. Parker, R.E. Port, J. Taylor, R.M. Weisskoff, Estimating kinetic parameters from dynamic contrast-enhanced T(1)-weighted MRI of a diffusable tracer: standardized quantities and symbols, J. Magn. Reson. Imaging. 10 (1999) 223–232, https://doi.org/10.1002/(SICI)1522-2586(199909)10:3%3C223::AID-JMRI2%3E3.0.CO;2-S.
[36] D.W. Workie, B.J. Dardzinski, Quantifying dynamic contrast-enhanced MRI of the knee in children with juvenile rheumatoid arthritis using an arterial input function (AIF) extracted from popliteal artery enhancement, and the effect of the choice of the AIF on the kinetic parameters, Magn. Reson. Med. 54 (2005) 560–568, https://doi.org/10.1002/mrm.20597.
[37] W. Huang, Y. Chen, A. Fedorov, X. Li, G.H. Jajamovich, D.I. Malyarenko, M.P. Aryal, P.S. LaViolette, M.J. Oborski, F. O'Sullivan, R.G. Abramson, K. Jafari-Khouzani, A. Afzal, A. Tudorica, B. Moloney, S.N. Gupta, C. Besa, J. Kalpathy-Cramer, J.M. Mountz, C.M. Laymon, M. Muzi, P.E. Kinahan, K. Schmainda, Y. Cao, T.L. Chenevert, B. Taouli, T.E. Yankeelov, F. Fennessy, X. Li, The impact of arterial input function determination variations on prostate dynamic contrast-enhanced magnetic resonance imaging pharmacokinetic modeling: a multicenter data analysis challenge, part II, Tomogr. (Ann Arbor, Mich.). 5 (2019) 99–109, https://doi.org/10.18383/j.tom.2018.00027.
[38] M. Boesen, O. Kubassova, M.A. Cimmino, M. Østergaard, P. Taylor, B. Danneskiold-Samsoe, H. Bliddal, Dynamic Contrast Enhanced MRI Can Monitor the Very Early Inflammatory Treatment Response upon Intra-Articular Steroid Injection in the Knee Joint: A Case Report with Review of the Literature, Arthritis 2011 (2011) 1–8, https://doi.org/10.1155/2011/578252.
[39] C.A. Cuenod, D. Balvay, Perfusion and vascular permeability: basic concepts and measurement in DCE-CT and DCE-MRI, Diagn. Interv. Imaging 94 (2013) 1187–1204, https://doi.org/10.1016/J.DIII.2013.10.010.
[40] T.J. Mosher, Z. Zhang, R. Reddy, S. Boudhar, B.N. Milestone, W.B. Morrison, C.K. Kwoh, F. Eckstein, W.R. Witschey, A. Borthakur, Knee articular cartilage damage in osteoarthritis: analysis of MR image biomarker reproducibility in ACRIN-PA 4001 multicenter trial, Radiology 258 (2011) 832–842, https://doi.org/10.1148/radiol.10101174.
[41] H. Shao, C. Pauli, S. Li, Y. Ma, A.S. Tadros, A. Kavanaugh, E.Y. Chang, G. Tang, J. Du, Magic angle effect plays a major role in both T1rho and T2 relaxation in articular cartilage, Osteoarthr. Cartil. 25 (2017) 2022–2030, https://doi.org/10.1016/j.joca.2017.01.013.
[42] A.T. Collins, M.L. Kulvaranon, H.C. Cutcliffe, G.M. Utturkar, W.A.R. Smith, C.E. Spritzer, F. Guilak, L.E. DeFrate, Obesity alters the in vivo mechanical response and biochemical properties of cartilage as measured by MRI, Arthritis Res. Ther. 20 (2018) 232, https://doi.org/10.1186/s13075-018-1727-4.
[43] K.A. Taylor, A.T. Collins, L.N. Heckelman, S.Y. Kim, G.M. Utturkar, C.E. Spritzer, W.E. Garrett, L.E. DeFrate, Activities of daily living influence tibial cartilage T1rho relaxation times, J. Biomech. 82 (2019) 228–233, https://doi.org/10.1016/j.jbiomech.2018.10.029.
[44] A. Bashir, M.L. Gray, R.D. Boutin, D. Burstein, Glycosaminoglycan in articular cartilage: in vivo assessment with delayed Gd(DTPA)(2-)-enhanced MR imaging, Radiology 205 (1997) 551–558, https://doi.org/10.1148/radiology.205.2.9356644.
[45] B. Herz, A. Albrecht, M. Englbrecht, G.H. Welsch, M. Uder, N. Renner, P. Schlechtweg, D. Paul, L. Lauer, K. Engelke, R. Janka, J. Rech, G. Schett, S. Finzel, Osteitis and synovitis, but not bone erosion, is associated with proteoglycan loss and microstructure damage in the cartilage of patients with rheumatoid arthritis, Ann. Rheum. Dis. 73 (2014) 1101–1106, https://doi.org/10.1136/annrheumdis-2012-202850.
[46] C.J. Tiderius, J. Sandin, J. Svensson, L.E. Dahlberg, L. Jacobsson, Knee cartilage quality assessed with dGEMRIC in rheumatoid arthritis patients before and after treatment with a TNF inhibitor, Acta radiol. 51 (2010) 1034–1037, https://doi.org/10.3109/02841851.2010.510482.
[47] T.J. Mosher, B.J. Dardzinski, Cartilage MRI T2 relaxation time mapping: overview and applications, Semin. Musculoskelet. Radiol. 08 (2004) 355–368, https://doi.org/10.1055/s-2004-861764.
[48] S.J. Matzat, E.J. McWalter, F. Kogan, W. Chen, G.E. Gold, T $_2$ Relaxation time quantitation differs between pulse sequences in articular cartilage, J. Magn. Reson. Imaging 42 (2015) 105–113, https://doi.org/10.1002/jmri.24757.
[49] B. Sveinsson, A.S. Chaudhari, G.E. Gold, B.A. Hargreaves, A simple analytic method for estimating T2 in the knee from DESS, Magn. Reson. Imaging 38 (2017) 63–70, https://doi.org/10.1016/j.mri.2016.12.018.
[50] G.H. Welsch, F.F. Hennig, S. Krinner, S. Trattnig, T2 and T2* mapping, Curr. Radiol. Rep. 2 (2014) 60, https://doi.org/10.1007/s40134-014-0060-1.
[51] S. Apprich, G.H. Welsch, T.C. Mamisch, P. Szomolanyi, M. Mayerhoefer, K. Pinker, S. Trattnig, Detection of degenerative cartilage disease: comparison of high-resolution morphological MR and quantitative T2 mapping at 3.0 Tesla, Osteoarthr. Cartil. 18 (2010) 1211–1217, https://doi.org/10.1016/J.JOCA.2010.06.002.
[52] T. Baum, G.B. Joseph, D.C. Karampinos, P.M. Jungmann, T.M. Link, J.S. Bauer, Cartilage and meniscal T2 relaxation time as non-invasive biomarker for knee osteoarthritis and cartilage repair procedures, Osteoarthr. Cartil. 21 (2013) 1474–1484, https://doi.org/10.1016/J.JOCA.2013.07.012.
[53] W.T. Dixon, Simple proton spectroscopic imaging, Radiology 153 (1984) 189–194, https://doi.org/10.1148/radiology.153.1.6089263.
[54] C.D.G. Hines, H. Yu, A. Shimakawa, C.A. McKenzie, J.H. Brittain, S.B. Reeder, T1 independent, T2* corrected MRI with accurate spectral modeling for quantification of fat: validation in a fat-water-SPIO phantom, J. Magn. Reson. Imaging 30 (2009) 1215–1222, https://doi.org/10.1002/jmri.21957.
[55] D.J. Tyler, M.D. Robson, R.M. Henkelman, I.R. Young, G.M. Bydder, Magnetic resonance imaging with ultrashort TE (UTE) PULSE sequences: technical considerations, J. Magn. Reson. Imaging 25 (2007) 279–289, https://doi.org/10.1002/jmri.20851.
[56] M. Weiger, D.O. Brunner, B.E. Dietrich, C.F. Müller, K.P. Pruessmann, ZTE imaging in humans, Magn. Reson. Med. 70 (2013) 328–332, https://doi.org/10.1002/mrm.24816.
[57] B. Chen, Y. Zhao, X. Cheng, Y. Ma, E.Y. Chang, A. Kavanaugh, S. Liu, J. Du, Three-dimensional ultrashort echo time cones (3D UTE-Cones) magnetic resonance imaging of entheses and tendons, Magn. Reson. Imaging 49 (2018) 4–9, https://doi.org/10.1016/j.mri.2017.12.034.
[58] M. Ostergaard, M. Stoltenberg, P. Lovgreen-Nielsen, B. Volck, S. Sonne-Holm, I. Lorenzen, Quantification of synovistis by MRI: correlation between dynamic and static gadolinium-enhanced magnetic resonance imaging and microscopic and macroscopic signs of synovial inflammation, Magn. Reson. Imaging 16 (1998) 743–754, https://doi.org/10.1016/S0730-725X(98)00008-3.
[59] M.B. Axelsen, M. Stoltenberg, R.P. Poggenborg, O. Kubassova, M. Boesen, H. Bliddal, K. Horslev-Petersen, L.G. Hanson, M. Ostergaard, Dynamic gadolinium-enhanced magnetic resonance imaging allows accurate assessment of the synovial inflammatory activity in rheumatoid arthritis knee joints: a comparison with synovial histology, Scand. J. Rheumatol. 41 (2012) 89–94, https://doi.org/10.3109/03009742.2011.608375.
[60] S. Vordenbaumen, C. Schleich, T. Logters, P. Sewerin, E. Bleck, T. Pauly, A. Muller-Lutz, G. Antoch, M. Schneider, F. Miese, B. Ostendorf, Dynamic contrast-enhanced magnetic resonance imaging of metacarpophalangeal joints reflects histological signs of synovitis in rheumatoid arthritis, Arthritis Res. Ther. 16 (2014) 452, https://doi.org/10.1186/s13075-014-0452-x.
[61] A.M. Barendregt, C.M. Nusman, R. Hemke, C. Lavini, D. Amiras, T.W. Kuijpers,

M. Maas, Feasibility of diffusion-weighted magnetic resonance imaging in patients with juvenile idiopathic arthritis on 1.0-T open-bore MRI, Skelet. Radiol. 44 (2015) 1805–1811, https://doi.org/10.1007/s00256-015-2208-3.
[62] F. Hilbert, A. Holl-Wieden, A. Sauer, H. Kostler, H. Neubauer, Intravoxel incoherent motion magnetic resonance imaging of the knee joint in children with juvenile idiopathic arthritis, Pediatr. Radiol. 47 (2017) 681–690, https://doi.org/10.1007/s00247-017-3800-6.
[63] M. Li, A. Sauer, A. Holl-Wieden, T. Pabst, H. Neubauer, Diagnostic value of diffusion-weighted MRI for imaging synovitis in pediatric patients with inflammatory conditions of the knee joint, World J. Pediatr. (2019), https://doi.org/10.1007/s12519-019-00232-8.
[64] J. Qu, X. Lei, Y. Zhan, H. Li, Y. Zhang, Assessing synovitis and bone Erosion With apparent diffusion coefficient in early stage of rheumatoid arthritis, J. Comput. Assist. Tomogr. 41 (2017) 833–838, https://doi.org/10.1097/RCT.0000000000000609.
[65] A.M. Barendregt, E.C. van Gulik, C. Lavini, C.M. Nusman, J.M. van den Berg, D. Schonenberg-Meinema, K.M. Dolman, T.W. Kuijpers, R. Hemke, M. Maas, Diffusion-weighted imaging for assessment of synovial inflammation in juvenile idiopathic arthritis: a promising imaging biomarker as an alternative to gadolinium-based contrast agents, Eur. Radiol. 27 (2017) 4889–4899, https://doi.org/10.1007/s00330-017-4876-y.
[66] T. Pap, A. Korb-Pap, Cartilage damage in osteoarthritis and rheumatoid arthritis—two unequal siblings, Nat. Rev. Rheumatol. 11 (2015) 606–615, https://doi.org/10.1038/nrrheum.2015.95.
[67] A. Korb-Pap, A. Stratis, K. Muhlenberg, B. Niederreiter, S. Hayer, F. Echtermeyer, R. Stange, J. Zwerina, T. Pap, H. Pavenstadt, G. Schett, J.S. Smolen, K. Redlich, Early structural changes in cartilage and bone are required for the attachment and invasion of inflamed synovial tissue during destructive inflammatory arthritis, Ann. Rheum. Dis. 71 (2012) 1004–1011, https://doi.org/10.1136/annrheumdis-2011-200386.
[68] H. Tsushima, K. Okazaki, Y. Takayama, M. Hatakenaka, H. Honda, T. Izawa, Y. Nakashima, H. Yamada, Y. Iwamoto, Evaluation of cartilage degradation in arthritis using T1rho magnetic resonance imaging mapping, Rheumatol. Int. 32 (2012) 2867–2875, https://doi.org/10.1007/s00296-011-2140-3.
[69] X.H. Meng, Z. Wang, L. Guo, X.C. Liu, Y.W. Zhang, Z.W. Zhang, X.L. Ma, Quantitative evaluation of knee cartilage and meniscus destruction in patients with rheumatoid arthritis using T1rho and T2 mapping, Eur. J. Radiol. 96 (2017) 91–97, https://doi.org/10.1016/j.ejrad.2017.09.018.
[70] J. Hirose, H. Nishioka, M. Tsukano, S. Matsubara, K. Usuku, H. Mizuta, Matrix changes in articular cartilage in the knee of patients with rheumatoid arthritis after biological therapy: 1-year follow-up evaluation by T2 and T1rho MRI quantification, Clin. Radiol. 73 (2018) 984 e11–984 e18, https://doi.org/10.1016/j.crad.2018.06.020.
[71] E. Ku, V. Pedoia, M. Tanaka, U. Heilmeier, J. Imboden, J. Graf, T. Link, X. Li, Evaluating radiocarpal cartilage matrix changes 3-months after anti-TNF treatment for rheumatoid arthritis using MR T1rho imaging, J. Magn. Reson. Imaging 45 (2016) 1514–1522, https://doi.org/10.1002/jmri.25448.
[72] J. Fransen, P.L.C.M. van Riel, The disease activity score and the EULAR response criteria, Rheum. Dis. Clin. North Am. 35 (2009) 745–757, https://doi.org/10.1016/j.rdc.2009.10.001 vii–viii.
[73] C. Buchbender, A. Scherer, P. Kropil, B. Korbl, M. Quentin, Dc. Reichelt, R.S. Lanzman, C. Mathys, D. Blondin, B. Bittersohl, C. Zilkens, M. Hofer, H.J. Wittsack, M. Schneider, G. Antoch, B. Ostendorf, F. Miese, Cartilage quality in rheumatoid arthritis: comparison of T2* mapping, native T1 mapping, dGEMRIC, DeltaR1 and value of pre-contrast imaging, Skelet. Radiol. 41 (2012) 685–692, https://doi.org/10.1007/s00256-011-1276-2.
[74] F.R. Miese, B. Ostendorf, H.J. Wittsack, D.C. Reichelt, T.C. Mamisch, C. Zilkens, R.S. Lanzman, M. Schneider, A. Scherer, Metacarpophalangeal joints in rheumatoid arthritis: delayed gadolinium-enhanced MR imaging of cartilage–a feasibility study, Radiology 257 (2010) 441–447, https://doi.org/10.1148/radiol.10100459.
[75] F. Miese, C. Buchbender, A. Scherer, H.J. Wittsack, C. Specker, M. Schneider, G. Antoch, B. Ostendorf, Molecular imaging of cartilage damage of finger joints in early rheumatoid arthritis with delayed gadolinium-enhanced magnetic resonance imaging, Arthritis Rheum. 64 (2012) 394–399, https://doi.org/10.1002/art.33352.
[76] N. Renner, G. Kronke, J. Rech, M. Uder, R. Janka, L. Lauer, D. Paul, B. Herz, P. Schlechtweg, F.F. Hennig, G. Schett, G. Welsch, Anti-citrullinated protein antibody positivity correlates with cartilage damage and proteoglycan levels in patients with rheumatoid arthritis in the hand joints, Arthritis Rheumatol. 66 (2014) 3283–3288, https://doi.org/10.1002/art.38862.
[77] C. Schleich, A. Muller-Lutz, P. Sewerin, B. Ostendorf, C. Buchbender, M. Schneider, G. Antoch, F. Miese, Intra-individual assessment of inflammatory severity and cartilage composition of finger joints in rheumatoid arthritis, Skelet. Radiol. 44 (2015) 513–518, https://doi.org/10.1007/s00256-014-2045-9.
[78] P. Sewerin, A. Muller-Lutz, D.B. Abrar, S. Odendahl, M. Eichner, M. Schneider, B. Ostendorf, C. Schleich, Prevention of the progressive biochemical cartilage destruction under methotrexate therapy in ear[1], in: L.A. Bradbury, K.A. Hollis, B. Gautier, S. Shankaranarayana, P.C. Robinson, N. Saad, K.-A.L.ê Cao, M.A. Brown (Eds.), Diffusion-Weighted Imaging Is a Sensitive a, Clin Exp Rheumatol, vol. 37, 2018, pp. 179–185 https://www.ncbi.nlm.nih.gov/pubmed/29998824.
[79] A.C. Kight, B.J. Dardzinski, T. Laor, T.B. Graham, Magnetic resonance imaging evaluation of the effects of juvenile rheumatoid arthritis on distal femoral weight-bearing cartilage, Arthritis Rheum. 50 (2004) 901–905, https://doi.org/10.1002/art.20062.
[80] N. Renner, A. Kleyer, G. Krönke, D. Simon, S. Söllner, J. Rech, M. Uder, R. Janka, G. Schett, G.H. Welsch, M.L. Pachowsky, T2 mapping as a new method for quantitative assessment of cartilage damage in RA, J. Rheumatol. (2019), https://doi.org/10.3899/jrheum.180728 jrheum.180728.
[81] H.K. Kim, T. Laor, T.B. Graham, C.G. Anton, S.R. Salisbury, J.M. Racadio, B.J. Dardzinski, T2 relaxation time changes in distal femoral articular cartilage in children with juvenile idiopathic arthritis: a 3-Year longitudinal study, Am. J. Roentgenol. 195 (2010) 1021–1025, https://doi.org/10.2214/AJR.09.4019.
[82] Z. Bozgeyik, S. Ozgocmen, E. Kocakoc, Role of diffusion-weighted MRI in the detection of early active sacroiliitis, Am. J. Roentgenol. 191 (2008) 980–986, https://doi.org/10.2214/AJR.07.3865.
[83] E. Gezmis, F.Y. Donmez, M. Agildere, Diagnosis of early sacroiliitis in seronegative spondyloarthropathies by DWI and correlation of clinical and laboratory findings with ADC values, Eur. J. Radiol. 82 (2013) 2316–2321, https://doi.org/10.1016/j.ejrad.2013.08.032.
[84] N. Gaspersic, I. Sersa, V. Jevtic, M. Tomsic, S. Praprotnik, Monitoring ankylosing spondylitis therapy by dynamic contrast-enhanced and diffusion-weighted magnetic resonance imaging, Skelet. Radiol. 37 (2008) 123–131, https://doi.org/10.1007/s00256-007-0407-2.
[85] L.A. Bradbury, K.A. Hollis, B. Gautier, S. Shankaranarayana, P.C. Robinson, N. Saad, K.-A.L.ê Cao, M.A. Brown, Diffusion-weighted imaging is a sensitive and specific magnetic resonance sequence in the diagnosis of ankylosing spondylitis, J. Rheumatol. 45 (2018) 771–778, https://doi.org/10.3899/jrheum.170312.
[86] T.J.P. Bray, K. Vendhan, N. Ambrose, D. Atkinson, S. Punwani, C. Fisher, D. Sen, Y. Ioannou, M.A. Hall-Craggs, Diffusion-weighted imaging is a sensitive biomarker of response to biologic therapy in enthesitis-related arthritis, Rheumatol. (United Kingdom). 56 (2017) 399–407, https://doi.org/10.1093/rheumatology/kew429.
[87] K.H. Lee, H.Y. Chung, X. Xu, V.W.H. Lau, C.S. Lau, Apparent diffusion coefficient as an imaging biomarker for spinal disease activity in axial spondyloarthritis, Radiology 291 (2019) 121–128, https://doi.org/10.1148/radiol.2019180960.
[88] B. Dallaudiere, R. Dautry, P.M. Preux, A. Perozziello, J. Lincot, E. Schouman-Claeys, J.M. Serfaty, Comparison of apparent diffusion coefficient in spondylarthritis axial active inflammatory lesions and type 1 Modic changes, Eur. J. Radiol. 83 (2014) 366–370, https://doi.org/10.1016/j.ejrad.2013.10.009.
[89] R.G. Lambert, W.P. Maksymowych, Diffusion-weighted imaging in axial spondyloarthritis: A measure of effusion or does it elicit confusion? J. Rheumatol. 45 (6) (2018) 729–730, https://doi.org/10.3899/jrheum.171479.
[90] A. Hall-Craggs, Bray MA, Ciurtin TJP, C. Bainbridge, Quantitative magnetic resonance imaging has potential for assessment of spondyloarthritis: arguments for its study and use, J. Rheumatol. 46 (2019) 541–542.
[91] T.J.P. Bray, A. Dudek, N. Sakai, K. Rajesparan, C. Fisher, C. Ciurtin, D. Sen, A. Bainbridge, M.A. Hall-Craggs, The BEACH tool: a Quantitative MRI-based method for measuring oedema and fat metaplasia in spondyloarthritis, EULAR (2018) 821, https://doi.org/10.1136/annrheumdis-2018-eular.4612.
[92] F. Wang, C. Chu, C. Zhao, Y. Wei, Q. Zhang, Q. Feng, W. Chen, J. He, L. Sun, Z. Zhou, Diffusion kurtosis imaging in sacroiliitis to evaluate the activity of ankylosing spondylitis, J. Magn. Reson. Imaging 49 (2018) 101–108, https://doi.org/10.1002/jmri.26194.
[93] T.J.P. Bray, A. Bainbridge, M. Hall-Craggs, H. Zhang, Intravoxel incoherent motion outperforms monoexponential and kurtosis models of diffusion attenuation in normal and inflamed bone marrow, ISMRM abstract (abstract 1361), (2019) online link: https://www.ismrm.org/19/program_files/DP01.htm.
[94] D. Hernando, S.D. Sharma, M. Aliyari Ghasabeh, B.D. Alvis, S.S. Arora, G. Hamilton, L. Pan, J.M. Shaffer, K. Sofue, N.M. Szeverenyi, E.B. Welch, Q. Yuan, M.R. Bashir, I.R. Kamel, M.J. Rice, C.B. Sirlin, T. Yokoo, S.B. Reeder, Multisite, multivendor validation of the accuracy and reproducibility of proton-density fat-fraction quantification at 1.5T and 3T using a fat–water phantom, Magn. Reson. Med. 77 (2017) 1516–1524, https://doi.org/10.1002/mrm.26228.
[95] M. Bainbridge, A Bray, T Sengupta, R Hall-Craggs, Comparison of Quantitative MRI Fat-Fraction measurement in the Sacroiliac Joint on different scanner platforms Intl Soc Mag Reson Med, 209AD.
[96] T.J.P. Bray, A. Bainbridge, S. Punwani, Y. Ioannou, M.A. Hall-Craggs, Simultaneous quantification of bone Edema/Adiposity and structure in inflamed bone using chemical shift-encoded MRI in spondyloarthritis, Magn. Reson. Med. 79 (2018) 1031–1042, https://doi.org/10.1002/mrm.26729.
[97] B.S. Koo, Y. Song, J.H. Shin, S. Lee, T.-H. Kim, Evaluation of disease chronicity by bone marrow fat fraction using sacroiliac joint magnetic resonance imaging in patients with spondyloarthritis: a retrospective study, Int. J. Rheum. Dis. 22 (2019) 734–741, https://doi.org/10.1111/1756-185X.13485.
[98] C. Ren, Q. Zhu, H. Yuan, Mono-exponential and bi-exponential model-based diffusion-weighted MR imaging and IDEAL-IQ sequence for quantitative evaluation of sacroiliitis in patients with ankylosing spondylitis, Clin. Rheumatol. 37 (2018) 3069–3076, https://doi.org/10.1007/s10067-018-4321-x.
[99] T.J.P. Bray, A. Karsa, A. Bainbridge, N. Sakai, S. Punwani, M.A. Hall-Craggs, K. Shmueli, Association of bone mineral density and fat fraction with magnetic susceptibility in inflamed trabecular bone, Magn. Reson. Med. 81 (2019) 3094–3107, https://doi.org/10.1002/mrm.27634.
[100] R.L. Janiczek, G. Gambarota, C.D.J. Sinclair, T.A. Yousry, J.S. Thornton, X. Golay, R.D. Newbould, Simultaneous T 2 and lipid quantitation using IDEAL-CPMG, Magn. Reson. Med. 66 (2011) 1293–1302, https://doi.org/10.1002/mrm.22916.
[101] J.M. Morrow, C.D.J. Sinclair, A. Fischmann, P.M. Machado, M.M. Reilly, T.A. Yousry, J.S. Thornton, M.G. Hanna, MRI biomarker assessment of neuromuscular disease progression: a prospective observational cohort study, Lancet Neurol. 15 (2015) 65–77, https://doi.org/10.1016/S1474-4422(15)00242-2.
[102] M. Zhang, L. Zhou, N. Huang, H. Zeng, S. Liu, L. Liu, Assessment of active and inactive sacroiliitis in patients with ankylosing spondylitis using quantitative dynamic contrast-enhanced MRI, J. Magn. Reson. Imaging 46 (2017) 71–78, https://

doi.org/10.1002/jmri.25559.
[103] W.C. Bae, S. Patil, R. Biswas, S. Li, E.Y. Chang, S. Statum, D.D. D'Lima, C.B. Chung, J. Du, Magnetic resonance imaging assessed cortical porosity is highly correlated with μCT porosity, Bone 66 (2014) 56–61, https://doi.org/10.1016/j.bone.2014.06.004.
[104] C.S. Rajapakse, M. Bashoor-Zadeh, C. Li, W. Sun, A.C. Wright, F.W. Wehrli, Volumetric Cortical Bone Porosity Assessment with MR Imaging: Validation and Clinical Feasibility, Radiology 276 (2015) 526–535, https://doi.org/10.1148/radiol.15141850.
[105] W.C. Bae, P.C. Chen, C.B. Chung, K. Masuda, D. D'Lima, J. Du, Quantitative ultrashort echo time (UTE) MRI of human cortical bone: correlation with porosity and biomechanical properties, J. Bone Miner. Res. 27 (2012) 848–857, https://doi.org/10.1002/jbmr.1535.
[106] G. Schett, R.J. Lories, M.A. D'Agostino, D. Elewaut, B. Kirkham, E.R. Soriano, D. McGonagle, Enthesitis: from pathophysiology to treatment, Nat. Rev. Rheumatol. 13 (2017) 731–741, https://doi.org/10.1038/nrrheum.2017.188.
[107] S.L. Hennigan, J. Du, C. Chung, G. Bydder, A. Kavanaugh, Evaluation of enthesopathy in psoriatic arthritis using a 3 T MRI and using novel ultrashort time echo pulse sequences for imaging, Am. Coll. Rheumatol. (December) (2007) 4252–4253 internal-pdf://0521140917/S-2007-Evaluation of enthesopathy in psoriatic.pdf.
[108] R.J. Hodgson, A.J. Grainger, P.J. O'Connor, R. Evans, L. Coates, H. Marzo-Ortega, P. Helliwell, D. McGonagle, P. Emery, M.D. Robson, Imaging of the Achilles tendon in spondyloarthritis: a comparison of ultrasound and conventional, short and ultrashort echo time MRI with and without intravenous contrast, Eur. Radiol. 21 (2011) 1144–1152, https://doi.org/10.1007/s00330-010-2040-z.
[109] R.J. Hodgson, N. Menon, A.J. Grainger, P.J. O'Connor, D. McGonagle, P. Helliwell, P. Emery, M.D. Robson, Quantitative MRI measurements of the Achilles tendon in spondyloarthritis using ultrashort echo times, Br. J. Radiol. 85 (2012) e293–9, https://doi.org/10.1259/bjr/13555456.
[110] E.T. Ahrens, J. Zhong, In vivo MRI cell tracking using perfluorocarbon probes and Fluorine-19 detection, NMR Biomed. 26 (2013) 860–871, https://doi.org/10.1002/nbm.2948.
[111] C. Jacoby, S. Temme, F. Mayenfels, N. Benoit, M.P. Krafft, R. Schubert, J. Schrader, U. Flögel, Probing different perfluorocarbons for in vivo inflammation imaging by 19F MRI: image reconstruction, biological half-lives and sensitivity, NMR Biomed. 27 (2014) 261–271, https://doi.org/10.1002/nbm.3059.
[112] J.D. MacKenzie, Y.-F. Yen, D. Mayer, J.S. Tropp, R.E. Hurd, D.M. Spielman, Detection of inflammatory arthritis by using hyperpolarized 13C-Pyruvate with MR imaging and spectroscopy, Radiology 259 (2011) 414–420, https://doi.org/10.1148/radiol.10101921.
[113] K. Yasaka, O. Abe, Deep learning and artificial intelligence in radiology: Current applications and future directions, PLoS Med. 15 (2018) e1002707, , https://doi.org/10.1371/journal.pmed.1002707.
[114] R. Hemke, C. Lavini, C.M. Nusman, J.M. van den Berg, K.M. Dolman, D. Schonenberg-Meinema, Ma J. van Rossum, T.W. Kuijpers, M. Maas, Pixel-by-pixel analysis of DCE-MRI curve shape patterns in knees of active and inactive juvenile idiopathic arthritis patients, Eur. Radiol. 24 (2014) 1686–1693, https://doi.org/10.1007/s00330-014-3168-z.